Chapter 19
Fabrication and Characterization of High-Performance Anti-reflecting Nanotextured Si Surfaces for Solar Cells

Stepan Nichkalo, Anatoly Druzhinin, Valeriy Yerokhov, and Oleksandr Ostapiv

19.1 Introduction

In the past decades, great efforts have been undertaken to develop various photovoltaic (PV) devices [1–11]. Today Si-based PV devices remain the basis of the current PV industry due to the abundance of Si materials and the high efficiency of Si solar cells [12]. However, the high reflective index of Si causes the reflection of more than 30% of incident light. As a result, the photoconversion efficiency of the Si-PV device greatly reduces. For traditional Si wafer-based solar cells, the pyramidal or inverted pyramidal structures were generally constructed on Si surface to reduce the reflection loss for incident light and to increase the light absorption [13, 14]. However, such microstructured surfaces are not able to reduce reflectance below 10% [15–18]. At the same time, the anti-reflecting coating layers, such as Si_3N_4, MgF_2, and Si_3N_4/MgF_2, are also applied to suppress light reflection of microstructured surface, but they suffer from destructive interference of reflected light and lead to a narrowing of the solar spectrum of absorbed photons, as a result [19–21]. In this regard, the nanotexturing of Si surface is widely studied to reach maximum values of the absorption coefficient and to reduce reflection in a wide spectral range, improving the efficiency of solar cells.

Among microstructures, Si nanowires (SiNWs) are also widely considered as an important class of nanoscale building blocks for high-performance devices due to their unique structural, electrical, and thermoelectric properties in addition to their compatibility with current Si-based microelectronics [22–33]. Recent studies on the optical characteristics of SiNWs demonstrate their promising applications in solar cell [34–40]. These nanostructures are long enough to absorb most of incident light, and their small diameters provide a short collection length for excited carriers in a

S. Nichkalo (✉) · A. Druzhinin · V. Yerokhov · O. Ostapiv
Lviv Polytechnic National University, Lviv, Ukraine

O. Fesenko, L. Yatsenko (eds.), *Nanooptics, Nanophotonics, Nanostructures, and Their Applications*, Springer Proceedings in Physics 210,
https://doi.org/10.1007/978-3-319-91083-3_19

direction normal to the light absorption [38, 41]. Additionally, unlike bulk Si with its indirect optical band gap of 1.12 eV and low absorption coefficient of 10^4/cm, the optical band gap of SiNWs can be varied between 1.1 eV and 3.5 eV by decreasing SiNW diameter between 7 nm and 1.3 nm, respectively [41, 42]. Several research groups showed that in the near ultraviolet-visible-near-infrared region, optical reflectance of SiNWs is one to two orders of magnitude lower than Si [43–47]. However, such structures are effective the best under direct sunlight illumination and could not face the sun at the appropriate angle from morning to evening [48, 49]. The use of sun-tracking systems for the purpose of receiving direct light illumination is not cost-effective for practical applications. The concept of a complex structure combining the advantages of pyramids and SiNWs might help to achieve the omnidirectional light absorption and overcome the directional dependence of PV performance [49]. Realization of this concept predicts utilizing of traditional alkaline texturing of Si wafer to produce the pyramidal Si and the metal-assisted chemical etching (MACE) to fabricate SiNWs on the side faces of pyramids. The use of MACE method for fabricating of SiNWs was motivated by its simplicity, good cost-efficiency, versatility, and ability to control various parameters, e.g. cross section, shape, diameter, length, and orientation [50, 51]. In contrast, the crystallographic orientation of SiNWs grown by vapour-liquid-solid (VLS) technique depends upon the diameter of nanowire [52, 53]. Moreover, the crystalline quality of SiNWs produced by MACE method generally is high, and their surfaces are typically rougher than VLS-grown NWs [50, 54]. In general, SiNWs prepared by MACE demonstrate higher solar cell performance over VLS-grown SiNWs [55].

Here we present experimental results on application of MACE method for fabricating different morphologies on the surface of Si wafer and the comparison of their optical properties in terms to develop photosensitive structures with low reflectivity and high light absorption over an extended solar spectral range.

19.2 Experimental Details

Single-crystalline *p*-type Si (100) and Si (111) wafers with resistivity of 0.3–1 $\Omega \times$ cm were chosen for experiments. The wafers were cut into square samples of 2×2 cm^2 and then sequentially cleaned in acetone, isopropyl alcohol (IPA), and deionized (DI) water for 20 min at room temperature. Afterwards, samples were dipped in the mixed solution of ammonium hydroxide NH_4OH (30%), hydrogen peroxide H_2O_2 (35%), and DI water H_2O with volumetric ratio v/v/v = 1/1/5 at 70 °C for 10 min to remove any organic residues. In order to obtain an efficient anti-reflecting surface with a maximum absorption and the least possible reflection for possible use in photovoltaics, three types of morphology of Si surface were made and examined, namely, (1) rough nanograss, (2) random pyramids, and (3) pyramids with nanotextured side faces.

Fabrication of the nanograss morphology was carried out through metal-assisted chemical etching of Si (111) wafer, accompanied by the following steps. At the first

stage, clean square Si wafer samples were dipped in a solution of 5 M HF and 2 mM $AgNO_3$ for 2 min at room temperature that resulted in a deposition of Ag particles on the Si surface. Then, samples were rinsed by DI water for 10 s and immersed in the etchant solution HF(40%) + H_2O_2(35%) + H_2O (v/v/v = 4/1/4) at room temperature for 10 min. After etching process, samples were immersed in a mixed solution of NH_4OH and H_2O_2 (v/v = 3/1) at room temperature for 10 min to remove Ag residues. Prepared samples were rinsed with DI water for 10 min and dried.

Random pyramids were fabricated by anisotropic etching of Si (100) wafer in a mixed solution of potassium hydroxide (KOH) (9 wt %) and acetic acid (5 vol %) at 75 °C for 10 min. The textured Si samples were then immersed in dilute hydrochloric acid (HCl) for 10 min and hydrofluoric acid (HF) for 5 min to remove any residue KOH and silicon dioxide, respectively. At the next, pyramid-textured Si samples were rinsed with DI water for 20 min at room temperature and dried.

For the nanotexturing of the side faces of Si pyramids, the MACE method was used. First, Ag particles were deposited on precleaned pyramid-textured Si wafers by immersing samples in a solution of 0.14 M HF and 0.5 mM $AgNO_3$ for 7 min at room temperature and then rinsed by DI water for 10 s. Low molar concentrations of HF and $AgNO_3$ were used in order to obtain well-defined and small seeds of Ag on the side faces of Si micropyramids. Subsequently, pyramid-textured Si samples covered by Ag nanoseeds were immersed in the mixed etching solution of HF (40%), H_2O_2(35%), and DI water (v/v/v = 4/1/4) at room temperature for 12 min. Finally, all the samples were immersed in a mixed solution NH_4OH + H_2O_2 (v/v = 3/1) at room temperature for 10 min to remove the residual Ag on the surface of the samples.

The surface of Si wafer was characterized by using a SELMI 106I scanning electron microscope (SEM). Optical spectra of the samples were measured by spectrophotometer at the wavelength ranging from 300 to 1100 nm.

19.3 Results and Discussion

Figure 19.1 shows the cross-section view SEM images of Si wafer after 10 min of Ag-assisted chemical etching in HF + H_2O_2 + H_2O solution at room temperature. As a result, vertically aligned SiNWs were formed on Si surface. As can be seen in Fig. 19.1a–b, the NWs are preferentially cone-shaped reminding a grass, with diameters ranging from 100 nm to 500 nm and an average height of about 4 μm.

Shown in Fig. 19.2a–b are the top-view and cross-section view SEM images of random Si pyramids formed as a result of etching of Si wafer in KOH-based solution at 75 °C for 10 min. As we see, the average size of pyramids does not exceed 5 μm.

Fig. 19.3 shows the top-view SEM image of pyramid-textured Si wafers with predeposited Ag nanoseeds after immersing samples in a solution of 0.14 M HF/0.5 mM $AgNO_3$ for 7 min at room temperature. Consequently, chemical treatment of pyramidal samples covered by Ag nanoseeds in etching solution of HF (40%)/H_2O_2(35%)/H_2O (v/v/v = 4/1/4) at room temperature for 12 min revealed to

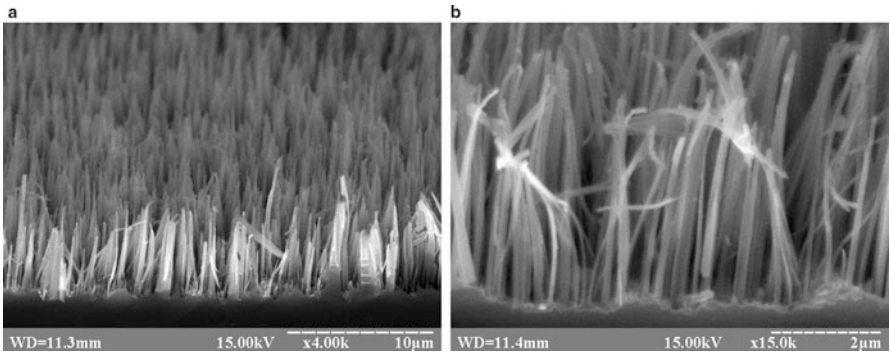

Fig. 19.1 Cross-section view SEM images of Si wafer after 10 min of Ag-assisted chemical etching in $HF/H_2O_2/H_2O$ (v/v/v = 4/1/4) solution at room temperature at different scale. (**a**) The scale 10 µm. (**b**) The scale 2 µm

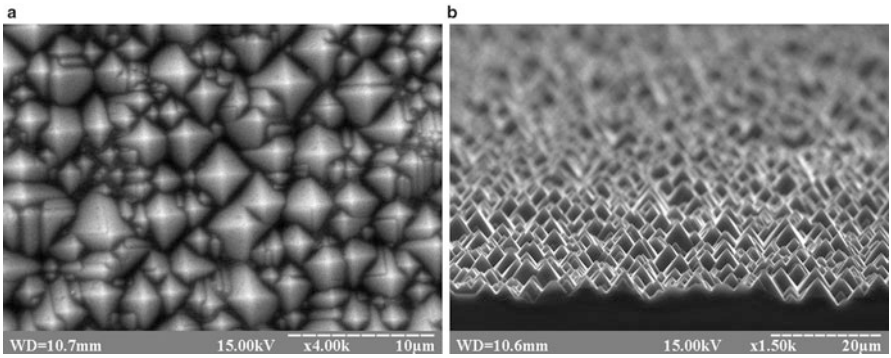

Fig. 19.2 SEM images of random Si pyramids formed as a result of etching of Si wafer in a solution of KOH (9%) and acetic acid (5%) at 75 °C for 10 min. (**a**) Top view. (**b**) Cross-section view

the formation of <111> − oriented SiNWs which were etched normally to the surface planes of Si pyramids (see Fig. 19.4a). As can be seen in Fig. 19.4b, the NWs are 325 nm in height with mean diameter about 130 nm.

The rough nanograss on micropyramids predicted to have a strong absorption and extremely low reflection ability. This suggestion is confirmed by experimental results of measurement of absorbance (Fig. 19.5a) and reflectance spectra (Fig. 19.5b) of Si wafer samples with various surface morphologies. It was found that in comparison to other textures, the pyramidal Si samples textured by Si nanograss demonstrate a highest value of light absorption, more than 98%, whereas for a non-textured Si wafer and a pyramid-textured Si, this value is found to be typical, 60% and 85%, respectively (Fig. 19.5a). The high absorption of Si nanograss, about 95%, could be explained in terms of specific nanowire geometry, which is conical (see Fig. 19.1b). According to [16], compared with planar thin film

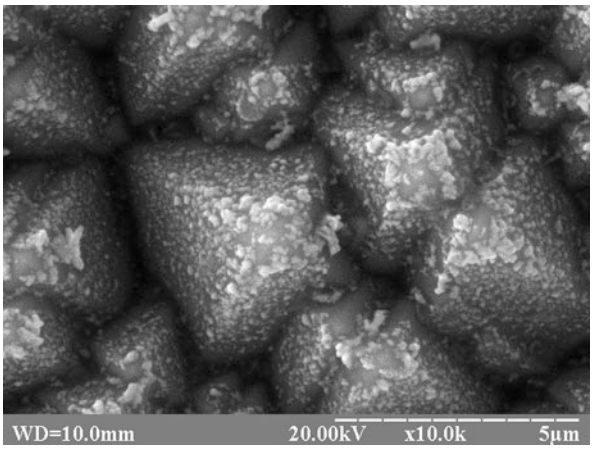

Fig. 19.3 Top-view SEM image of pyramidal Si wafer with deposited Ag nanoseeds after immersing samples in a solution of 0.14 M HF/0.5 mM $AgNO_3$ for 7 min at room temperature

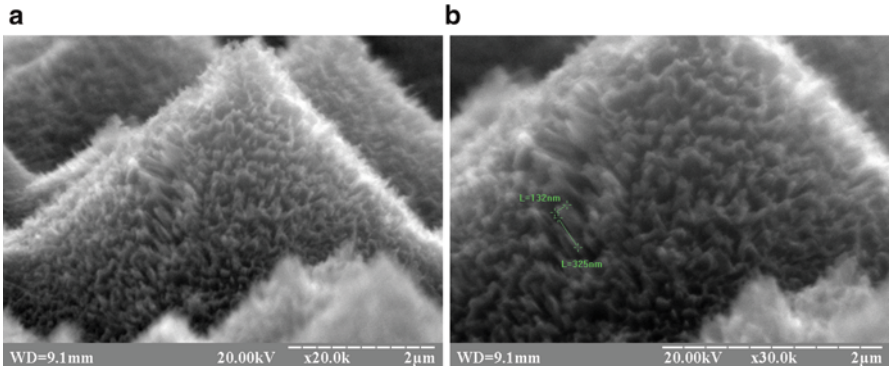

Fig. 19.4 Cross-section view SEM images of Si micropyramids nanotextured by Si nanograss after etching in HF(40%)/H_2O_2(35%)/H_2O (v/v/v = 4/1/4) at room temperature for 12 min. (**a**) General view of the pyramid. (**b**) Scaled-up view of the side face of a pyramid with SiNWs

and NWs with uniform diameters, the cone-shaped Si nanostructures show improved absorption because of a gradual increase of the effective refractive index from the Si surface to air. From another hand, in aperiodic SiNWs, absorption at long-wavelength regime is not degraded, unlike periodic NWs, in which calculated absorptance for early band edge photons dwarfs due to the significant transmission loss [56]. In their work [56], authors showed that optimization of aperiodic NWs by using a random walk algorithm reveals to an over 100% enhancement factor in PV efficiency compared to the periodic counterparts.

Figure 19.5b compares the optical reflection between pyramid-textured Si, Si nanograss, and Si pyramids with a nanograss texture of side faces of pyramids. In contrast to pyramid-textured Si and Si nanograss, the Si pyramids with a nanograss texture possess a lowest reflection ability (< 1%) in all optical spectral range of wavelength. For the record, the low reflection value (about 4%) was observed for Si

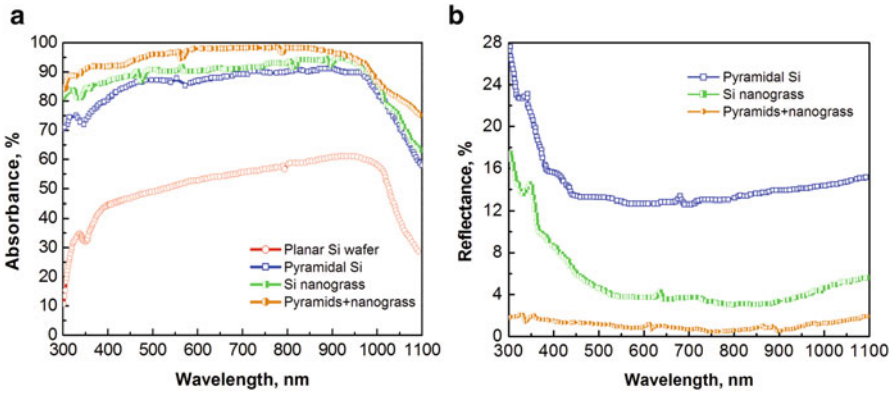

Fig. 19.5 (**a**) Absorbance spectra for pyramid-textured Si, Si nanograss, complex structure Si pyramids+Si nanograss, and planar Si wafer (serve as reference). (**b**) Reflectance spectra for pyramid-textured Si, Si nanograss, complex structure Si pyramids+Si nanograss

nanograss as well. These findings confirm the accusation that vertically aligned NWs with random position or diameter can also achieve similar low reflectance and high absorption as the ordered NWs with uniform diameter [57]. In their work [57], authors showed that the random diameters of the nanowire arrays can lead to different broadened resonant frequencies which give rise to absorption enhancement. While the absorption at the original off-resonance frequency is enhanced, the original resonance frequency maintains high, caused by multiple scattering induced by the random arrangement or diameter of NWs. In other words, aperiodic Si NWs demonstrate suppression of light reflection similar to the random pyramid texture. Thus, almost the same behaviour of a reflection dependence for Si nanograss and pyramidal Si samples is observed (see Fig. 19.5b).

19.4 Conclusions

It was demonstrated that the metal-assisted chemical etching is a simple, versatile, and flexible method, which can be successfully utilized for fabrication of Si nanostructures on the surface of Si wafer with good anti-reflecting properties. By using this method, an array of SiNWs and a complex Si structure composed of Si pyramids, obtained by conventional alkali chemical etching, and SiNWs prepared on the side faces of pyramids have been produced on Si wafers. It was found that Si micropyramids textured by a rough SiNWs with an average diameter of 130 nm, and 325 nm in height, show a strong absorption and extremely low reflection ability. In particular, the absorbance of pyramidal Si samples textured by Si nanograss was more than 98% and reflectance less than 1% in all range of wavelength (300–1100 nm), whereas for a non-textured Si wafer and a pyramid-textured Si,

these values were found to be typical. The low reflection value (about 4%) was also observed for Si nanograss. Such nanostructured surfaces in the form of Si micropyramids and SiNWs might exhibit better omnidirectional light-trapping ability by multiple reflections resulting in enhanced optical characteristics and will find a wide variety of significant applications in solar cells, photodetectors, and optoelectronic devices.

References

1. Chapin DM, Fuller CS, Pearson GL (1964) A new silicon p-n junction photocell for converting solar radiation into electrical power. J Appl Phys 25:676
2. Green MA (2001) Crystalline silicon photovoltaic cells. Adv Mater 13:1019–1022
3. Goetzberger A, Hebling C, Schock HW (2003) Photovoltaic materials, history, status and outlook. Mater Sci Eng R 40:1–46
4. Swanson RM (2006) A vision for crystalline silicon photovoltaics. Prog Photovolt 14:443–453
5. Zhao J, Wang A, Green MA, Ferrazza F (1998) 19.8% efficient "honeycomb" textured multicrystalline and 24.4% monocrystalline silicon solar cells. Appl Phys Lett 73:1991–1993
6. Knechtli RC, Loo RY, Kamath GS (1984) High-efficiency GaAs solar cells. IEEE Trans Electron Devices 31:577–588
7. Tanabe K (2009) A review of ultrahigh efficiency III-V semiconductor compound solar cells: multijunction tandem, lower dimensional, photonic up/down conversion and plasmonic nanometallic structures. Energies 2:504–530
8. Hoppe H, Sariciftci NS (2004) Organic solar cells: an overview. J Mater Res 19:1924–1945
9. Yerokhov V, Ierokhova O (2016) Improved porous silicon-based multifunctional materials for the solar cells antireflection coating. 2016 International Conference on Electronics and Information Technology, EIT 2016 – Conference Proceedings, pp 49–52
10. Yerokhov V, Ierokhova O (2016) Coatings of the black-silicon type for silicon solar cells. Modern problems of radio engineering, telecommunications and computer science, Proceedings of the 13th International Conference on TCSET 2016, pp 388–391
11. Kim JY, Lee K, Coates NE, Moses D, Nguyen TQ, Dante M, Heeger AJ (2007) Efficient tandem polymer solar cells fabricated by all-solution processing. Science 317:222–226
12. Peng K, Xu Y, Wu Y, Yan Y, Lee ST, Zhu J (2005) Aligned single-crystalline Si nanowire arrays for photovoltaic applications: review. Small 1(11):1062–1067
13. Sun CH, Min WL, Linn NC, Jiang P, Jiang B (2007) Templated fabrication of large area subwavelength antireflection gratings on silicon. Appl Phys Lett 91:231105
14. Chu AK, Wang JS, Tsai ZY, Lee CK (2009) A simple and cost-effective approach for fabricating pyramids on crystalline silicon wafers. Sol Energy Mater Sol Cells 93:1276–1280
15. Wang HP, Lai KY, Lin YR, Lin CA, He JH (2010) Periodic Si nanopillar arrays fabricated by colloidal lithography and catalytic etching for broadband and omnidirectional elimination of Fresnel reflection. Langmuir 26:12855–12858
16. Han SE, Chen G (2010) Toward the Lambertian limit of light trapping in thin nanostructured silicon solar cells. Nano Lett 10(11):4692–4696
17. Wang FY, Yang QD, Xu G et al (2011) Highly active and enhanced photocatalytic silicon nanowire arrays. Nanoscale 3:3269–3276
18. Lin H, Xiu F, Fang M et al (2014) Rational design of inverted nanopencil arrays for cost-effective, broadband and omnidirectional light harvesting. ACS Nano 8:3752–3760
19. Wang HP, Lin TY, Tsai ML et al (2014) Toward efficient and omnidirectional n-type Si solar cells: concurrent improvement in optical and electrical characteristics by employing microscale hierarchical structures. ACS Nano 8:2959–2969

20. Peng KQ, Lee ST (2011) Silicon nanowires for photovoltaic solar energy conversion. Adv Mater 23:198–215
21. Parida B, Choi J, Lim G, Park S, Kim K (2014) Formation of nanotextured surfaces on microtextured Si solar cells by metal-assisted chemical etching process. J Nanosci Nanotechnol 14(12):9224–9231
22. Cui Y, Wei QQ, Park HK, Lieber CM (2001) Nanowire nanosensors for highly sensitive and selective detection of biological and chemical species. Science 293:1289–1292
23. Maryamova I, Druzhinin A, Lavitska E, Gortynska I, Yatzuk Y (2000) Low temperature semiconductor mechanical sensors. Sens Actuators A Phys 85:153–157
24. Druzhinin A, Lavitska E, Maryamova I (1999) Medical pressure sensors on the basis of silicon microcrystals and SOI layers. Sens Actuators B Chem 58:415–519
25. Cui Y, Zhong ZH, Wang DL, Wang WU, Lieber CM (2003) High performance silicon nanowire field effect transistors. Nano Lett 3:149–152
26. Peng KQ, Jie JS, Zhang WJ, Lee ST (2008) Silicon nanowires for rechargeable lithium-ion battery anodes. Appl Phys Lett 93:033105
27. Goldberger J, Hochbaum AI, Fan R, Yang PD (2006) Silicon vertically integrated nanowire field effect transistors. Nano Lett 6:973–977
28. Chen LJ (2007) Silicon nanowires: the key building block for future electronic devices. J Mater Chem 17:4639
29. Druzhinin A, Ostrovskii I, Kogut I (2006) Thermoelectric properties of Si-Ge whiskers. Mater Sci Semicond Process 9:853–857
30. Zheng G, Patolsky F, Cui Y, Wang WU, Lieber CM (2005) Multiplexed electrical detection of cancer markers with nanowire sensor arrays. Nat Biotechnol 23:1294–1301
31. Chan CK, Peng HL, Liu G, McIlwrath K, Zhang XF, Huggins RA, Cui Y (2008) High-performance lithium battery anodes using silicon nanowires. Nat Nanotechnol 3:31–35
32. Hochbaum A, Chen R, Delgado RD, Liang W, Garnett EC, Najarian M, Majumdar A, Yang P (2008) Enhanced thermoelectric performance of rough silicon nanowires. Nature 451:163–167
33. Druzhinin A, Ostrovskii I, Kogut I, Nichkalo S, Shkumbatyuk T (2011) Si and Si-Ge wires for thermoelectrics. Phys Status Solidi C 8(3):867–870
34. Fang H, Li X, Song S, Xu Y, Zhu J (2008) Fabrication of slantingly-aligned silicon nanowire arrays for solar cell applications. Nanotechnology 19:255703
35. Garnett EC, Yang P (2008) Silicon nanowire radial p−n junction solar cells. J Am Chem Soc 130:9224–9225
36. Kelzenberg MD, Turner-Evans DB, Kayes BM, Filier MA, Putnam MC, Lewis NS, Atwater HA (2008) Photovoltaic measurements in single-nanowire silicon solar cells. Nano Lett 8:710–714
37. Stelzner T, Pietsch M, Andra G, Falk F, Ose E, Christiansen S (2008) Silicon nanowire-based solar cells. Nanotechnology 19:295203
38. Druzhinin AA, Yerokhov VY, Nichkalo SI, Berezhanskyi YI, Chekaylo MV (2015) Texturing of the silicon substrate with nanopores and Si nanowires for anti-reflecting surfaces of solar cells. J Nano Electron Phys 7(2):02030-1–02030-6
39. Zhu J, Yu Z, Burkhard GF, Hsu CM, Connor ST, Xu Y, Wang Q, McGehee M, Fan S, Cui Y (2008) Optical absorption enhancement in amorphous silicon nanowire and nanocone arrays. Nano Lett 9:279–282
40. Li J, Yu H, Wong SM, Zhang G, Sun X, Lo PGQ, Kwong DL (2009) Si nanopillar array optimization on Si thin films for solar energy harvesting. Appl Phys Lett 95:033102
41. Ramanujam J, Shiri D, Verma A (2011) Silicon nanowire growth and properties: a review. Mater Express 1(2):105–126
42. Ma DDD, Lee CS, Au FCK, Tong SY, Lee ST (2003) Small-diameter silicon nanowire surfaces. Science 299:1874–1877
43. Tsakalakos L, Balch J, Fronheiser J, Korevaar BA, Sulima O, Rand J (2007) Silicon nanowire solar cells. Appl Phys Lett 91:233117

44. Tsakalakos L, Balch J, Fronheiser J, Shih MY, LeBoeuf SF et al (2007) Strong broadband optical absorption in silicon nanowire films. J Nanophoton 1:013552
45. Druzhinin A, Yerokhov V, Nichkalo S, Berezhanskyi Y (2016) Micro- and nanotextured silicon for antireflective coatings of solar cells. J Nano Res 39:89–95
46. Nichkalo S, Druzhinin A, Evtukh A, Bratus' O, Steblova O (2017) Silicon nanostructures produced by modified MacEtch method for antireflective Si surface. Nanoscale Res Lett 12:106
47. Li X, Li J, Chen T, Tay BK, Wang J, Yu H (2010) Periodically aligned Si nanopillar arrays as efficient antireflection layers for solar cell applications. Nanoscale Res Lett 5:1721–1726
48. Kelzenberg MD, Boettcher SW, Petykiewicz JA et al (2010) Enhanced absorption and carrier collection in Si wire arrays for photovoltaic applications. Nat Mater 9:239–244
49. Pei Z, Hu H, Li S, Ye C (2017) Fabrication of orientation-tunable Si nanowires on silicon pyramids with omnidirectional light absorption. Langmuir 33(15):3569–3575
50. Huang Z, Geyer N, Werner P, de Boor J, Gösele U (2011) Metal-assisted chemical etching of silicon: a review. Adv Mater 23:285–308
51. Han H, Huang Z, Lee W (2014) Metal-assisted chemical etching of silicon and nanotechnology applications. Nano Today 9:271–304
52. Schmidt V, Senz S, Gösele U (2005) Diameter-dependent growth direction of epitaxial silicon nanowires. Nano Lett 5:931–935
53. Druzhinin AA, Ostrovskii IP (2004) Investigation of Si-Ge whiskers growth by CVD. Phys Status Solidi C 1(2):333–336
54. Druzhinin A, Evtukh A, Ostrovskii I, Khoverko Y, Nichkalo S, Dvornytskyi S (2015) Technological approaches for growth of silicon nanowire arrays. Springer Proc Phys 156:301–307
55. Yuan G, Aruda K, Zhou S, Levine A, Xie J, Wang D (2011) Understanding the origin of the low performance of chemically grown silicon nanowires for solar energy conversion. Angew Chem Int Ed 50:2334–2338
56. Lin C, Povinelli ML (2011) Optimal design of aperiodic, vertical silicon nanowire structures for photovoltaics. Opt Express 19:A1148–A1154
57. Bao H, Ruan X (2010) Optical absorption enhancement in disordered vertical silicon nanowire arrays for photovoltaic applications. Opt Lett 35:3378–3380